REPORT TITLE	DOCUMENT NUMBER
WISE Payload Image Quality	SDL/09-258
PREPARED BY	**DATE**
Mark Larsen	August 18, 2009
DISTRIBUTION: John Elwell, Valerie Duval, Ingolf Heinrichsen	

1. INTRODUCTION

This report describes the image quality analysis, results and conclusions of the WISE image quality ground verification. Several reports have been written that either relate to or provide input into this analysis. These include:

SDL/09-215 WISE Scanner linearity analysis

SDL/09-157 WISE focus Verification

SDL/09-308 WISE band 1 image quality post-vibe

The WISE band 1 image quality has the least margin of all 4 bands, and is the most sensitive to errors relating to image quality. For that reason, this report will focus mainly on band 1.

The layout of this report is as follows: First, Sections 2 and 3 provide background of the WISE instrument and image quality requirements. Section 4 provides details of the optical system components. Section 5 provides an overview of optics testing done both at SSG and at SDL. Section 6 describes two models used for WISE image quality analysis. Section 7 describes how the model and measurements are combined to obtain an on-orbit prediction of both payload performance and flight system performance. Section 8 provides a summary of the results.

2. BACKGROUND

Wide-field Infrared Survey Explorer (WISE) is a cost-capped MIDEX program funded by NASA's SMD Universe Division, managed by the Jet Propulsion Laboratory (JPL), and led by Principal Investigator Edward Wright from UCLA. The WISE

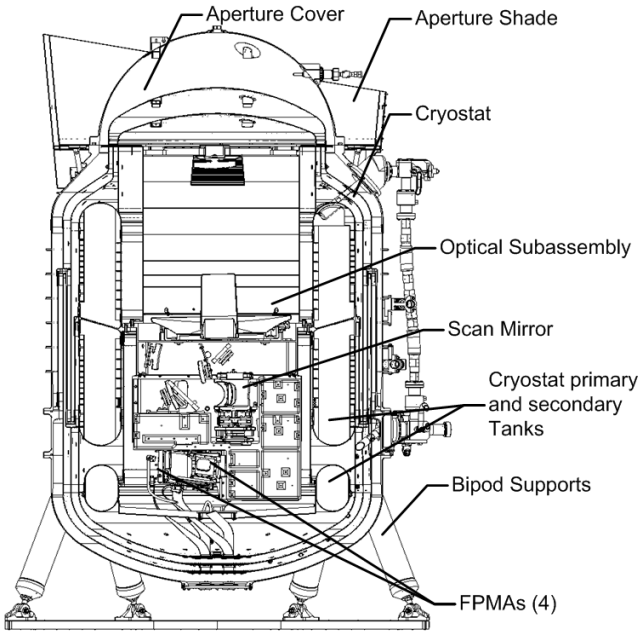

Figure 1: Payload cut-away view showing major components

mission will map the entire sky from 2.8 to 26 μm with sensitivity unmatched by any previous survey mission, achieving over 500,000 times the sensitivity of Cosmic Background Explorer (COBE) at 3.5 and 4.7 μm and a thousand times that of Infrared Astronomical Satellite (IRAS) at 12 and 25 μm. WISE will establish an essential database for testing theories of the origins of planets, stars, and galaxies and is a precursor for the James Webb Space Telescope (JWST).

The WISE science payload will operate in a single mode, continuously imaging portions of the sky as the sun-synchronous , 530-km orbit precesses around the celestial sphere. Following a month of in-orbit checkout, the all-sky survey will take 6 months to complete. Each focal plane, with a 1024x1024 pixel array and 2.75 arc second pixels, will cover a 47 arc minute field of view. The payload includes a cryogenic scan mirror to offset the orbital motion and freeze the sky during each 11 second frame—an 8.8 second integration time, plus 1.1 seconds each for readout and mirror flyback. Data will be processed using a sample up-the-ramp[1] technique.

The orbit precesses in ecliptic longitude by 1 degree per day or 4 arc minutes per orbit. The minimum number of exposures for any point on the sky is 8, accounting for a 10% frame-to-frame overlap and a 90% orbit-to-orbit overlap and planned outages for the moon, SAA, data downlink, and other outage events.

3. REQUIREMENTS

WISE image quality is measured in noise pixels[2]. Noise pixels describe the way detector noise leads to uncertainty in the measurement of the irradiance of a source. Under the assumption that the noise on all pixels is the same, and that the irradiance is estimated using a least squares fit of the source to an accurate point response function (PRF), the uncertainty in the irradiance of a source is

$$\sigma_F^2 = \sigma_S^2 N_p ,$$

where σ_F^2 is the variance of the irradiance estimate, and σ_S^2 is the variance of the detector noise, and the number of noise pixels, N_p is

$$N_p = \frac{\left(\sum V_{i,j}\right)^2}{\Omega \sum V_{i,j}^2} ,$$

where $V_{i,j}$ is the value of the PRF at location i, j, and Ω is the ratio of the detector size to the sample spacing of V. The sums are over all pixels containing power from a point source. Note that N_p is a function only of the PRF shape.

Noise pixels can also be calculated from the MTF:

$$N_p = \frac{1}{\Omega_{det} \int\int \Phi(f_x, f_y)^2 df_x df_y} ,$$

where, for WISE, $\Omega_{det} = (2.75 \text{ arcsec})^2$.

3.1 PAYLOAD

The payload image quality requirement is:

3.1.2.2 Image Quality {FRD 481}
The average payload image quality allocation across the optical FOV, excluding the corners shall be as shown in Table 3-1, assuming a 2.75-arcsec pixel.

Table 3-1: WISE Science Payload Noise Pixels

BAND		REQUIREMENT (UNITLESS)
1	2.8-3.8 µm	11.8
2	4.1-5.2 µm	15.4
3	7.5-16.5 µm	43.3
4	20-det. cutoff	130.8

The worst case payload image quality across the optical FOV, excluding the corners, shall not exceed the average payload image quality allocation by more than 20%.

The average image quality in a band shall be calculated at the center wavelength, which is defined as the average of the cut-on and cut-off wavelengths. Cut-on and cut-off wavelengths are defined, respectively, as the lowest and highest wavelengths in each band at which the product of the transmission and detector QE is 50% of their peak product.

The corner is defined as the region more than 0.95*sqrt[(L/2)^2 + (W/2)^2] from the center of the array, where L and W are the dimensions of the array (i.e., 1016 active pixels) projected on the sky.

For L = W = 46 arcmin, this would allow the minimum image quality requirement to be exceeded about 1.5 arcmin in from the corners.

3.2 SPACECRAFT

The spacecraft image quality requirement is:

L2FRD-482 The average spacecraft image quality allocation shall be 1.2 noise pixels for all Bands assuming a 2.75 arcsec pixel.

Spacecraft allocation is independent of spectral band and includes 20% margin

3.3 FLIGHT SYSTEM

The flight system image quality requirement is:

L2FRD-115 The average WISE flight system image quality, across the FOV excluding the corners shall be no greater than 14.5, 18.2, 48.4, and 136.0 noise pixels for Bands 1, 2, 3, and 4, respectively, assuming a 2.75 arcsec pixel. The worst case image quality across the optical FOV excluding the corners shall not exceed the average image quality requirement by more than 20%.

*Image quality defined in noise pixels is a way to roll disparate error sources into a single error value. Exclusion of corners is defined as regions more than 0.915*sqrt[(L/2)^2+((W/2)^2] from the center of the array, where L and W are the dimensions of the array (i.e., 1016 active pixels) projected on the sky. For L = W = 46 arcmin, this would allow the*

4. OPTICS OVERVIEW

4.1 OPTICAL SUBASSEMBLY

The WISE optical subassembly (see Figure 2) includes an afocal telescope, a scan mirror, imaging optics, and the beamsplitter assembly (BSA). The afocal telescope, scan mirror, and imaging optics were designed and fabricated by L-3 SSG-Tinsley, while SDL designed and fabricated the beamsplitter assembly (BSA). The optical subassembly mounts into the cryostat and is structurally and thermally tied to the cryostat via the interface flange. The scan mirror is placed in collimated space between the afocal optics and the imaging optics and holds the field of view steady on the sky as the spacecraft rotates in its orbit. Parameters of the optical subassembly are shown in Table 2.

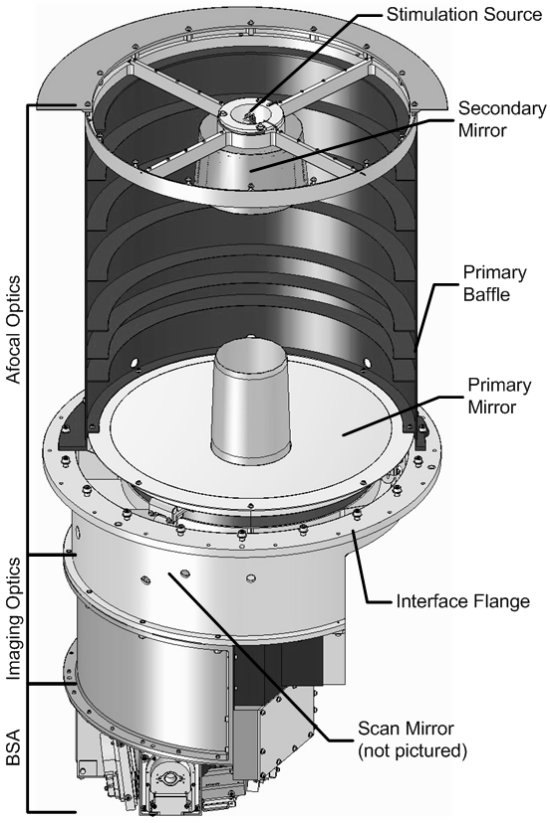

Figure 2: Optical subassembly

4.1.1 Telescope

Table 2: Key optical subassembly parameters

PARAMETER	PERFORMANCE
Field of View	46.9 x 46.9 arc minutes (0.783 x 0.783 degrees)
Field of Regard	46.9 x 86 arc minutes (0.783 x 1.433 degrees)
Focal length	1.35 m (53.15 inches)
Aperture diameter	40 cm (15.75 inches)
F#	3.375
Obscuration	19.4% by area
Afocal module	Number of mirrors: 6 Magnification: 8

Imager module	Number of mirrors: 6
Imager Field of View	6.264 x 6.264 degrees
Scan mirror (flat)	Scan range (adjustable): 25' to 39' (object space) or 100' to 156 ' (shaft angle) Retrace time: < 1.1 sec.
Operating temperature	< 17 K

The telescope is a 13-mirror, all-aluminum system that uses gold-coated, bare-polished aluminum mirrors. The cryogenic scan mirror is placed in collimated space between the afocal telescope and the imaging optics. The optics operate at less than 17 K to keep the instrument background low. Since the telescope was designed to be modular, the afocal optics, imaging optics, and scan mirror were developed and tested in parallel.

An important design constraint for the afocal telescope is its low distortion design. Because the scanner is placed in the beam after the afocal telescope, any distortion or scanner non-linearity causes a point source to wander on the focal plane during a scan, decreasing image quality.

4.1.2 Beam splitter assembly

The BSA is an aluminum structure that holds three beam splitters that separate the light from the imager into the four bands. The optical layout for the BSA is shown in Figure 3. The BSA provides the physical interface between the imager and the focal planes.

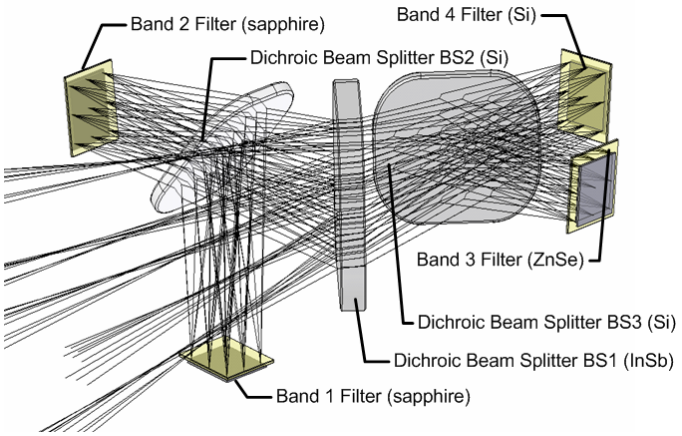

Figure 3: Beam splitter assembly

Composite thermal isolators are used between the FPMA mounts for bands 3 and 4 and the BSA, providing the thermal isolation needed to achieve the lower temperatures for the two Si:As FPAs, which are thermally strapped to the primary tank. Heaters are provided so these FPAs can be annealed on orbit, if necessary.

Filters are mounted as close as possible to each FPA to increase out-of-band rejection and reduce ghosting and the Stierwalt effect. Filters for bands 1 and 2 use a sapphire substrate. The band 3 filter uses ZnSe, and Band 4 uses a Silicon substrate.

5. OPTICS IMAGE QUALITY TEST RESULTS

5.1 SUMMARY OF IMAGING MODULE AND AFOCAL MODULE TESTING

Testing of the telescope was performed at SSG prior to shipment to SDL. The original intent was to perform a final test of the wavefront of the end-to-end reflective optical system, however

throughput was not sufficient to allow a double pass test.[1] Instead, a double pass measurement was made on the imaging module and afocal module separately.

Both the imaging module and the afocal module were tested at cryogenic temperatures, however due to high thermal loading in the test setup for the afocal, the afocal was only tested as a component down to 100K. The imager was tested at operating temperature (less than 20K).

See documents SSG01098 and SSG01099 for details of the testing completed at SSG.

5.1.1 Measured Wavefront

5.1.1.1 Imager

Results of the imager testing are contained in SSG document SSG01098. The imager was tested at approximately 15 K at 5 field points within the WISE imager field of view. The RMS wavefront error at those 5 positions is shown in Figure 4. Note that the on-axis point had test errors associated with the test fixture.

0.44		0.25
	0.56	
0.44		0.41

Figure 4: Wavefront (RMS at 0.6328 μm) at various positions within the WISE Imager FOV. These wavefronts were measured at 15 K

Compared to the pre-vibe wavefront, the imager changed by approximately 0.114 waves RMS at HeNe using using surface map subtraction[2].

The change in wavefront from the first cold cycle to the second was measured to be 0.07 waves RMS at HeNe using surface map subtraction. This change was measured at 15 K.

5.1.1.2 Afocal

The afocal was only tested to 100 K due to high thermal loading in the test setup. Rather than spend time and money fixing the test setup, the program elected to accept delivery of the system as it was. The wavefront measured at 3 field points at 100 K is shown in Figure 5.

The warm afocal wavefront changed by approximately 0.055 waves RMS at 0.633 μm from pre-vibe testing to post-vibe testing using surface map subtraction.

The afocal ambient wavefront change before and after a cryo-cycle was measured to be 0.094 waves RMS using surface map subtraction. This measurement is a warm-to-warm measurement, rather than a cryo-to-cryo measurement.

[1] The protective over coat on the gold coated aluminum mirrors was optimized for long wavelength transmission which lead to lower throughput at 0.633 μm than at first anticipated.

[2] Surface map subtraction is a conservative method for accounting for this change because the change reflected using surface map subtraction could be high even though the overall RMS wavefront error of the system may be the same.

0.384		0.395
	0.35	

Figure 5: Wavefront (RMS at 0.6328 μm) at various positions within the WISE afocal FOV. These were measured at 100 K

5.2 SUMMARY BSA RESULTS

The BSA assembly was tested cold, and both before and after a shake. Detailed results are reported in SDL/07-463. As shown in Figures 6 and 8 of SDL/07-463 the cold surface flatness of BS1 was measured to be essentially the same in two consecutive cool-downs. For the remainder of this section, 633nm waves are used as the unit of measure. The measured surface flatness error for BS1 was 0.593 waves PV (0.090 waves RMS) in the first cool down and 0.529 PV (0.084 waves RMS) in the second cool down. As can been seen from these figures, the high and low areas of the surface were in the same locations in both cool downs, so the surface subtraction was extremely small. As can be seen from Figures 13 and 14 of SDL/07-463, the surface flatness of BS1 before shaking was 0.785 waves PV (0.096 waves RMS) and 0.693 waves PV (0.111) waves after shaking. However, as can be seen from comparing Figures 13 and 14 the high and low areas changed places due to shaking. Consequently, the surface map subtraction was relatively large (0.898 waves PV and 0.170 waves RMS) as shown in Figure 15 of SDL/07-463.

Due to the design of the BSA, only BS1 could be observed in the shake induced surface flatness change test and the cryo-cycling test. The other beamsplitters, BS2 and BS3 are mounted similarly to BS1 but they are much smaller and hence have much smaller preloads. Room temperature surface flatness measurements on BS2 and BS3 and cryogenic surface flatness measurements on the uncoated BS2 and BS3 substrates showed the flatness errors were significantly smaller and tapping showed them to be much more stable with vibration than BS1. So the wavefront error effects of BS2 and BS3 are predicted to be negligible compared to the other contributors. Since surface flatness errors of BS1 are much greater when used in reflection as in Bands 1 and 2 than when used in transmittance as in Bands 3 and 4, the change in wavefront for bands 3 and 4 due to shaking was worst cased at one-half the change in Bands 1 and 2. The effect of these shake induced changes and cryo cycling errors on all 4 bands is included in the results described in Section 7.3.

5.3 MEASURED IMAGE QUALITY FROM BLUE TUBE TEST

Focus and image quality were measured post-vibe using the blue-tube configuration. This configuration is illustrated in Figure 6. In this configuration, a 300 inch collimator is used to present a point-like object to WISE. The blue tube shares the vacuum space with WISE, and has a fused silica window at one end, and is attached to WISE at the other. There is a LN2 cooled radiation shield that limits the heat load into the aperture of WISE while allowing observation of an external collimated source. The focal length of the collimator is 300”, and the diameter of the pinhole is 50 μm.

Using data taken in this configuration, the WISE image quality was found to be 10.7 noise pixels, as described in SDL/09-308. This image quality includes optics wavefront errors, detector and detector crosstalk, effects from the pinhole (50 µm aperture) and wavefront errors from the warm window and mylar filter.

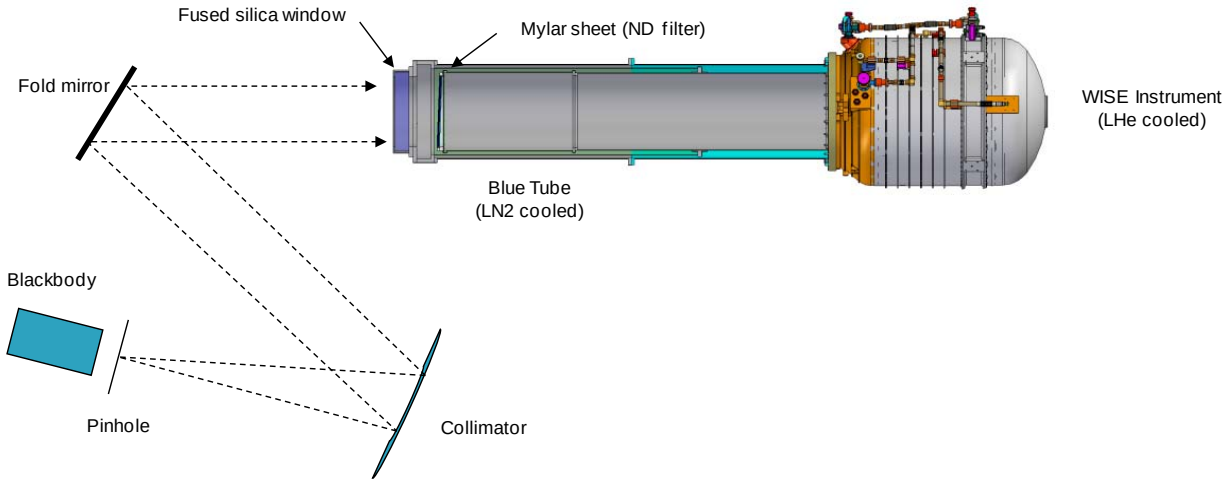

Figure 6: Blue tube configuration. This configuration was used to measure image quality and focus for Wise band 1.

6. MODELING

Two models were used in the analysis of image quality for WISE. The primary model is discussed next (Section 6.1), and is referred to as the parametric image quality model. The other model is discussed in Section 6.2 and is referred to as the WISE as-built wavefront model, which was used to correlate the parametric image quality model.

6.1 PARAMETRIC IMAGE QUALITY MODEL

The parametric image quality model was created early in the program to aid in trade studies and requirement flow down. This model incorporates the optics wavefront, aperture geometry (excluding the secondary spiders), detector effects, streak effects, and spacecraft effects. These effects are combined in the MTF domain and noise pixels are calculated from the MTF. Because of its ease of use and ability to model all the bands, it is also used for the on-orbit prediction of image quality. The remainder of Section 6.2 discusses the parametric image quality model.

6.1.1 Optics

6.1.1.1 Diffraction

The optics are modeled using the O'neil model for the MTF of a circular aperture with an obscuration, and the Hufnagle equation for design and fabrication wavefronts as shown below.

Let ϵ be the diameter ratio of the central obscuration to the total aperture and ν be the normalized frequency. Define the following functions

$$\phi(\epsilon,\nu) = \arccos\left(\frac{1+\epsilon^2-4\nu^2}{2\epsilon}\right),$$

$$A(\epsilon,\nu)=\frac{2}{\pi}\left(\arccos(\nu)-\nu\sqrt{1-\nu^2}\right),$$

$$B(\epsilon,\nu)=\begin{cases}\dfrac{2\epsilon^2}{\pi}\left(\arccos\left(\dfrac{\nu}{\epsilon}\right)-\sqrt{1-\left(\dfrac{\nu}{\epsilon}\right)^2}\right) & \text{if } \dfrac{\nu}{\epsilon}\le 1\\ 0 & \text{otherwise}\end{cases},$$

$$C(\varepsilon,\nu):=\begin{cases}-2\cdot\varepsilon^2 \text{ if } 0\le\nu\le\dfrac{1-\varepsilon}{2}\\ \dfrac{2}{\pi}\cdot\left[\varepsilon\cdot\sin(\phi(\varepsilon,\nu))+\dfrac{\phi(\varepsilon,\nu)}{2}\cdot\left(1+\varepsilon^2\right)-\left(1-\varepsilon^2\right)\cdot\operatorname{atan}\left(\dfrac{1+\varepsilon}{1-\varepsilon}\cdot\tan\left(\dfrac{\phi(\varepsilon,\nu)}{2}\right)\right)\right]-2\cdot\varepsilon^2 \text{ if } \dfrac{1-\varepsilon}{2}<\nu<\dfrac{1+\varepsilon}{2}\\ 0 \text{ if } \nu\ge\dfrac{1+\varepsilon}{2}\end{cases}$$

then the diffraction limited MTF is

$$\Phi_{Diff}(\epsilon,\nu)=\frac{A(\epsilon,\nu)+B(\epsilon,\nu)+C(\epsilon,\nu)}{1-\epsilon^2}.$$

6.1.1.2 Wavefront Errors and Defocus

The MTF due to design residuals, fabrication errors, and defocus is modeled using the Hufnagle equation,

$$\Phi_{wavefront}(\nu)=e^{-(2\pi W_{rms})^2\left(1-e^{-2n^2\nu^2}\right)},$$

where W_{rms} is the number of RMS waves of error, n is the number of Hufnagle "bumps", ν is the normalized frequency, and $\Phi_{wavefront}(\nu)$ is the MTF.

W_{rms} is the RSS sum of the wavefronts due to design residuals, fabrication errors, and defocus. Wavefront due to defocus is modeled using:

$$W_{defocus}=\frac{\Delta_{defocus}}{8\sqrt{12}F^2\lambda_c}$$

Where $\Delta_{defocus}$ is the defocus, F is the F# (3.375 for WISE), λ_c is the center wavelength for the band, and $W_{defocus}$ is the RMS wavefront error due to defocus.

6.1.2 Detector

The FPMA pixels have an 18 µm pitch, p, which with a focal length of 1.35 m results in a 2.75 arc-second square pixel. Since the pixels are square, the ideal pixel would have an MTF

$$\Phi_{ideal\_detector}(f_x, f_y) = \mathrm{sinc}(f_x p)\mathrm{sinc}(f_y p).$$

Unfortunately, the pixels in all 4 bands have crosstalk. Crosstalk can occur either due to inter-pixel capacitance, or due to a sample not completely settling before the next sample is taken.

Let x be the crosstalk; i.e., given that the response on a pixel is a, then the response on an adjacent (non-diagonal) pixel due to cross-talk is $x\,a$. The detector MTF with crosstalk, $\Phi_{detector}$, is modeled using

$$\Phi_{detector}(f_x, f_y, x) = \Phi_{crosstalk}(f_x, f_y, x)\Phi_{ideal\_detector}(f_x, f_y),$$

where

$$\Phi_{crosstalk}(f_x, f_y, x) = \frac{1 + 2x\left(\cos(2\pi f_x p) + \cos(2\pi f_y p)\right)}{1 + 4x}$$

Based on measurements of the autocorrelation function, this crosstalk is estimated to be approximately 3% in all directions for band 1.

6.1.3 Streak effects

Streaks include anything that causes a pixel to wander during a scan. For the payload, these include

- Non-linearity in the scan mirror
- Distortion in the afocal optics
- Scanner misalignment (includes angle to the shaft and flex pivot misalignments)

Spacecraft pointing errors can also cause streaks. Modeling of Spacecraft errors is described in Section 6.2.4.

In order to account for these effects, the current image quality model makes use of measurements made during MIC2 “scanner linearity” testing.

In these tests, we use MIC2 pointing mirror to simulate the motion of the spacecraft, while freezing the frame on the sky using the WISE scanner. This is done using a point-like source and moving the MIC2 pointing mirror a fixed angle, and then moving the WISE scanner a fixed angle in the opposite direction. This is done at 5 scanner angles over a 5x5 grid of field points. In the analysis, the optimal scanner “rate” and the optimal “yaw” angle is found and the extracted point source positions moved appropriately to compensate.

The wander of the point source over the scan is modeled by convolving the wander observed in the scanner linearity data with the PRF calculated using the parametric image quality model. Because the data includes all payload scan-modulated effects (streak effects), these measurements provide a good estimate of what will be observed on-orbit. These measurements and analyses are documented in SDL/09-215.

Because WISE is sampled using the sample up the ramp (SUR) technique, the weight associated with each part of the point source trajectory is not constant. The method for obtaining the kernel used in the convolution is described below.

WISE is sampled using the sample up the ramp (SUR) technique. For bands 1 and 2, WISE uses $N = 8$ samples up the ramp with coefficients $c = [-7, -5, -3, -1, 1, 3, 5, 7]$, and for bands 3 and 4, it uses $N = 9$ samples up the ramp with coefficients $c = [-4, -3, -2, -1, 0, 1, 2, 3, 4]$. To apply the SUR technique, the focal plane is reset, then each pixel is read out N times non-destructively. Define the value read from a single pixel in the array to be d_i, where $i = 1 \ldots N$. The algorithm returns

$$M = \frac{1}{S}\left(K + \sum_{i=1}^{N} c_i d_i \right), \tag{1}$$

where K is a constant offset added to the sum to avoid problems when the sum is slightly negative and S is a scale factor to prevent overflow.

We desire an estimate of the slope of d_i, since the slope is proportional to the power incident on the focal plane. Thus, the coefficients c_i are chosen so that M is proportional to a least squares estimate of the slope of d_i over i as described in [1].

Different parts of the integration time are weighted differently using this algorithm. Defining δ_i as the signal integrated between sample $i-1$ and i, (δ_1 is the offset on the pixel at the time of first sample) then clearly $d_i = \sum_{j=1}^{i} \delta_j$. By substitution into (1),

$$M = \sum_{i=1}^{N} \sum_{j=1}^{i} c_i \delta_j$$

which can be re-written

$$M = \sum_{j=1}^{N} \delta_j \sum_{i=j}^{N} c_i .$$

From this equation, it is clear that the weight given to δ_j is

$$w_j = \sum_{i=j}^{N} c_j . \tag{2}$$

For bands 1 and 2, $w = [0, 7, 12, 15, 16, 15, 12, 7]$ and for bands 3 and 4, $w = [4, 7, 9, 10, 10, 9, 7, 4]$.

Streak effects cause a point source to wander slightly on the array as the scanner moves through its range. Given that the relative position of the point source at time t within a scan is described by the trajectory $p(t) = \left[f_x(t), f_y(t) \right]$, the effect of this wander on the PRF is described by a convolution of the PRF with $w(t)\,p(t)$ where $w(t)$ is given by (2) for the integration time j containing time t.

The trajectory $p(t)$ was estimated over a 5x5 grid of field points using MIC2 measurements, as documented in SDL/09-215. The kernels $w(t)\,p(t)$ used in the convolution are shown in Figure 7. The title of each image is the increase in noise pixels caused by $w(t)\,p(t)$ in band 1for each of the 5x5 field points. These estimates are conservative because the actual wander will be smaller than indicated in the charts due to MIC2 pointing errors and point source extraction errors. The units of the horizontal and vertical axes are pixels. The appendix shows larger plots of the kernals at each location.

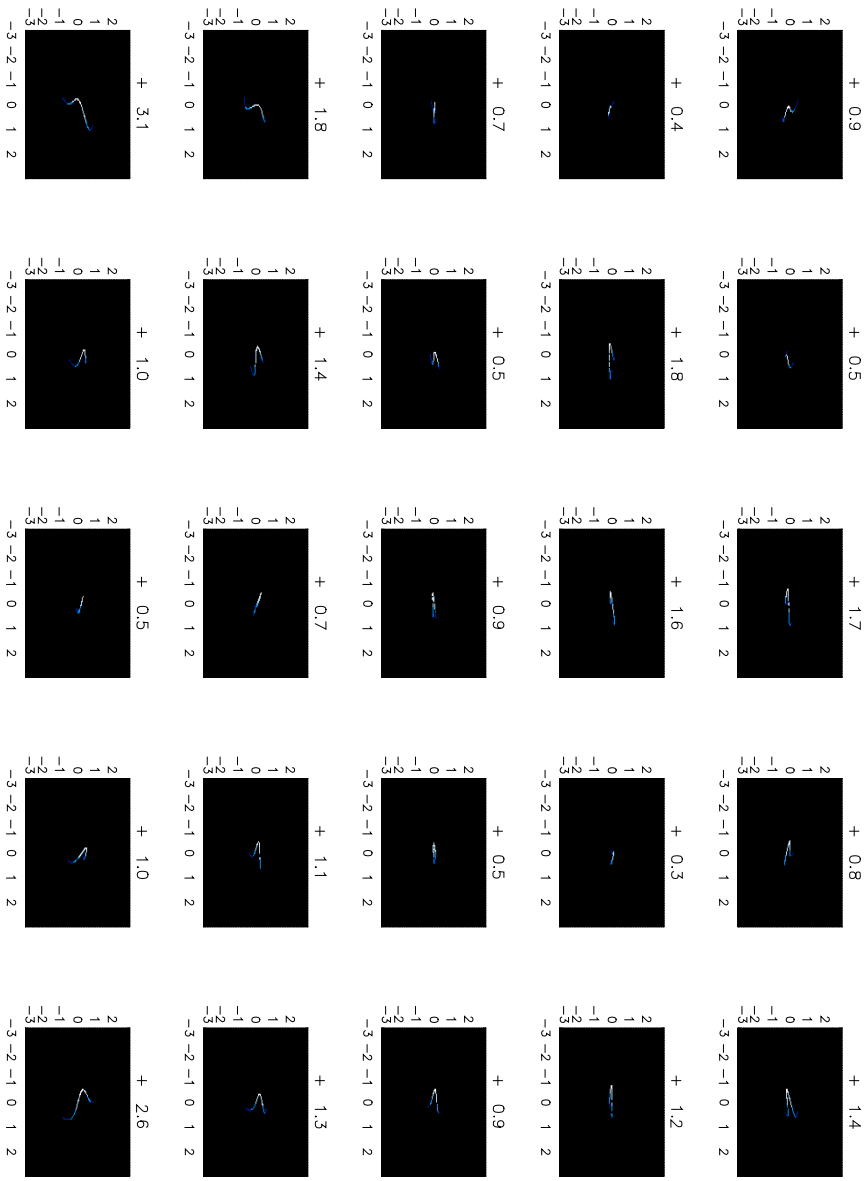

Figure 7: Streak trajectories $p(t)$ over the field of regard. The number in the title of each plot shows the effect of the streak on the image quality of the flight system for band 1. The color indicates the weight $w(t)$. The horizontal and vertical axes have units of pixels on the focal plane.

6.1.4 Spacecraft

The spacecraft contributes to image quality in several ways which are described in the following sub-sections.

The spacecraft coordinate system is defined as illustrated in Figure 8. The orbit is polar sun-synchronous, with its solar panel pointed towards the sun. Depending upon whether it's in an A.M. orbit or a P.M. orbit, it's direction of travel will be either in the $+x$ or $-x$ direction.

Rotations about the axes are named as if WISE were an airplane traveling in the x direction. Specifically, a rotation about the x axis is a roll, about y is pitch, and about z is yaw.

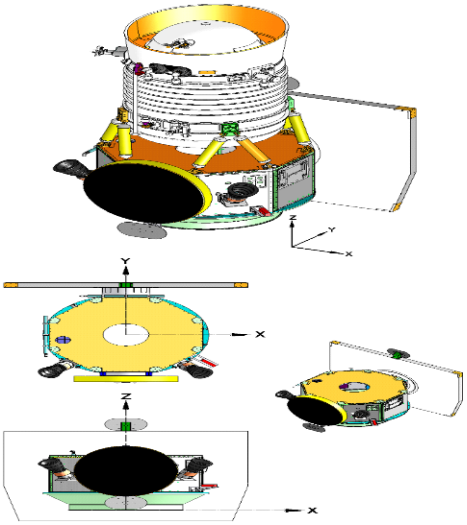

Figure 8: Spacecraft coordinate system definition

Pitch and roll jitter

Pitch and roll jitter directly affect image quality. This is modeled as a Gaussian blur:

$$\Phi_{jitter}(f,\sigma) = e^{-2\pi^2 f^2 \sigma^2 fl_{wise}^2},$$

Where σ is the magnitude of the jitter (angular standard deviation), and fl_{WISE} is the WISE focal length.

Yaw jitter

Because the yaw axis is a rotation about the boresight, image quality is not as sensitive to yaw jitter as it is to jitter about pitch or roll. Figure 9 illustrates the effect of yaw jitter on a source near the edge of the field. This effect is modeled conservatively using $\Phi_{jitter}(f,\sigma_{yaw}s)$, where s is 0.015 radians (50 arcminutes).

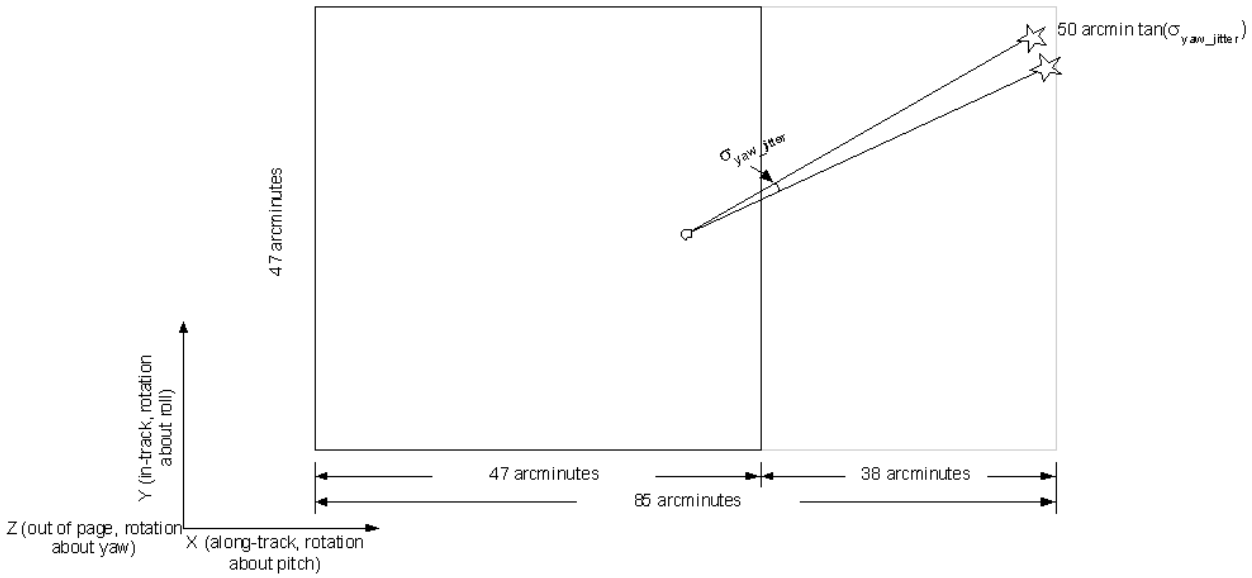

Figure 9: illustration showing the effect of spacecraft yaw jitter on image quality

Yaw misalignment

The effect of yaw misalignment on image quality is illustrated in Figure 10. Any misalignment in yaw causes the star to drift during a scan. Since the length of the scan, θ_{scan}, is 38 arc minutes (0.011 rad), the amount of drift d_{yaw} is θ_{scan} multiplied by the tangent of the yaw misalignment.

This is modeled using

$$\Phi_{ym}(f_y) = \text{sinc}(f_y \theta_{scan} \tan(\theta_{yaw\_mis})\, fl_{WISE}).$$

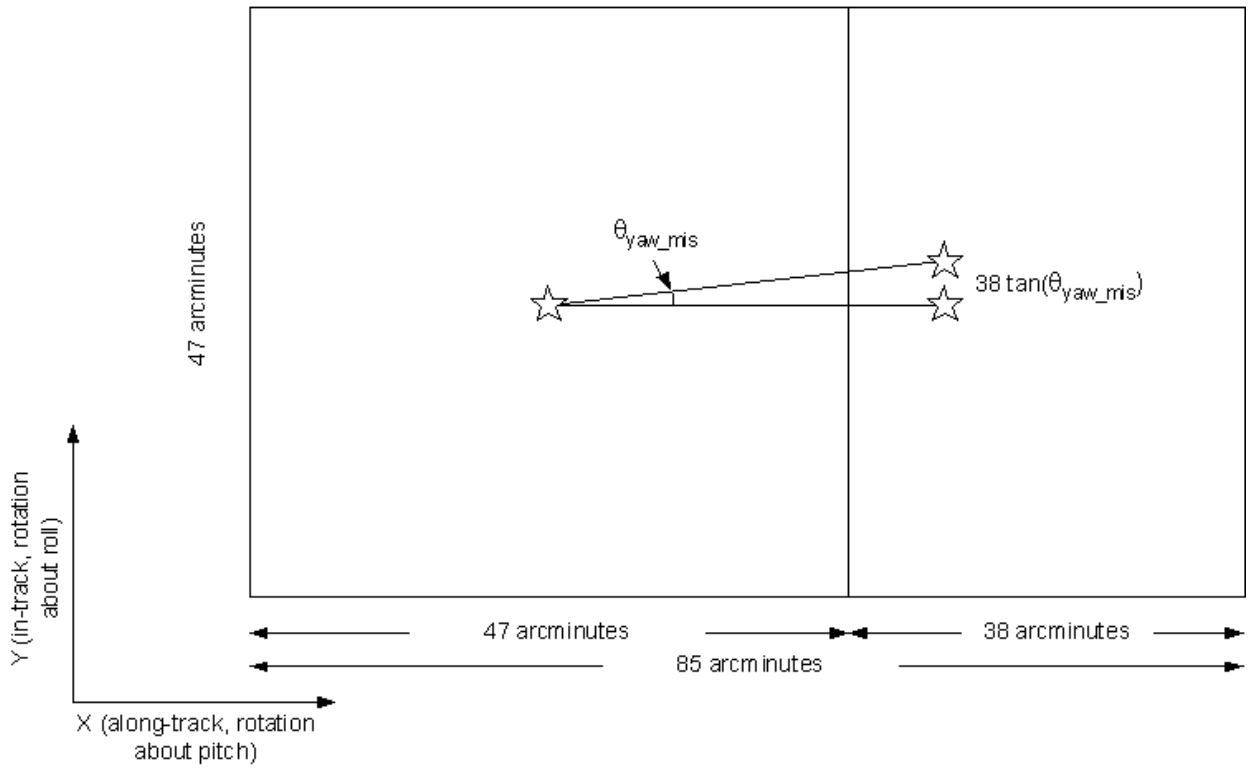

Figure 10: Illustration of the effect of yaw misalignment on image quality. A star moves $38\tan\left(\theta_{yaw\_mis}\right)$ arc-minutes over a scan

Pitch rate drift, Pitch rate and pitch rate estimate error
The pitch rate error is the error in the commanded rate of the spacecraft, the pitch rate estimate error is the error in estimating the correct pitch rate, and the pitch rate drift is the drift in the pitch rate. These all result in the same effect: a streak in the x axis of the image.

The length of the streak is the error $\delta\omega_{pitch}$ multiplied by the integration time of the focal planes, t_{int}. The pitch rate error is modeled using

$$\Phi_{pitch}(f_x) = \mathrm{sinc}(f_x\ \delta\omega_{pitch}\ t_{int}).$$

Roll rate drift
The roll rate drift is the drift in the roll rate, and is modeled similarly.

6.2 WISE AS-BUILT WAVEFRONT MODEL

An optical model of WISE was generated using component level measurements of the optical subsystems. This model will be referred to as the as-built wavefront model, and is described in the documents listed in Table 3.

Table 3: Documents describing the as-built wavefront model

"Apertures and Obscurations used in WISE and MIC2 Code V models"	SDL/09-444

"Attachment of Interferogram INT files in WISE and MIC2 as-built Code V models"	SDL/09-445
"Afocal field points and orientation for wavefront error tests"	SDL/09-446
"Imager Field Points and Orientation for cryogenic wavefront error test"	SDL/09-447

The parametric image quality model discussed in Section 6.1 was correlated to the as-built wavefront model as described below.

The as-built wavefront model was used to estimate the number of noise pixels that would be obtained in band 1 for various amounts of defocus, and thus wavefront, as shown in Table 3. The parametric model was then correlated with the as-built model by adjusting the number of Hufnagle bumps from 4 to 3.8, which obtains a better match of WFE to noise pixels near the WISE RMS WFE of 0.15 waves.

Table 4: Band 1 noise pixels vs. RMS WFE

Distance inside focus	RMS WFE	Noise Pixels
(inches)	(waves)	(#)
0	0.0977	6.494
0.001	0.1011	6.691
0.002	0.1084	7.155
0.003	0.1189	7.928
0.004	0.1318	9.065
0.005	0.1465	10.668
0.006	0.1626	12.814
0.007	0.1795	15.578

To improve the correlation between the parametric model and the as-built wavefront model at longer wavelengths, the as-built wavefront model was used to predict the image quality for band 4, which is dominated by diffraction effects. The image quality predicted by the as-built wavefront model is 27.45 noise pixels for a wavefront error of 0.0183 waves (RMS at 24 μm). The parametric model was correlated to the as-built model by adjusting the size of the obscuration from 16.5% (size of the central obscuration) to 19%.

7. IMAGE QUALITY PRE-LAUNCH ANALYSIS

The final image quality is obtained using the steps listed below.

7.1 BLUE TUBE WAVEFRONT

The analysis described in SDL/09-308 found that during blue tube test 5, the image quality for the optical system was approximately 10.7 noise pixels. This is the number of noise pixels

including the effect of the pinhole and aberrations from the GSE collimator, but excluding the Gaussian component, caused by jitter.

To determine the image quality of WISE, the parametric image quality model was modified to add the effect of the 50 µm aperture. This model was used to determine the wavefront error as a function of the blue tube image quality is shown in Figure 11. Evaluating this curve at 10.7 noise pixels results in a wavefront error of 0.1454 waves RMS at 3.3 µm. Subtracting the wavefront error due to the MIC3 collimator setup (0.042 waves RMS at 3.3 µm) results in an estimate of 0.139 waves RMS at 3.3 µm for the WISE wavefront error during blue tube test 5.

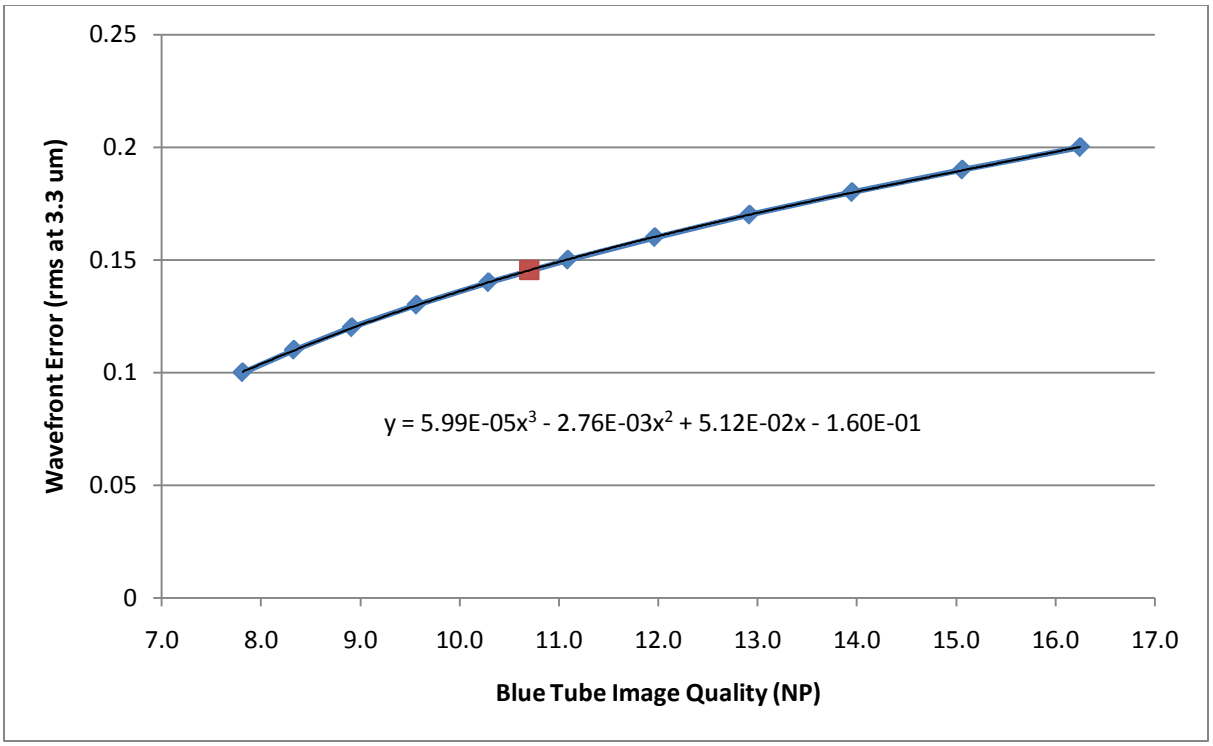

Figure 11: Image quality vs. Wavefront error in the blue tube configuration. The model accounts for, and removes the effect of, the 50 µm aperture used to illuminate the collimator. The operating point during the post-vibe blue tube test is highlighted.

7.2 ON-ORBIT WAVEFRONT

The flight system will undergo additional cryo-cycles, and one more shake during launch. To be conservative, the change in wavefront measured during component level tests as a result of cryo-cycling and shake was then added to the blue-tube wavefront (0.725 waves at HeNe) to obtain the on-orbit prediction of wavefront error. These wavefront changes are measured using surface-map subtraction, again adding some conservatism. The values used are shown in Table 3.

The resulting prediction of on-orbit wavefront is 0.804 waves RMS at HeNe (0.154 waves RMS at 3.3 µm). The afocal and imager are all-reflective, thus achromatic. Using the predicted design and fabrication residuals based on measurements of the BSA components, bands 2, 3, and 4 have 0.88, 1.06, 1.16 waves RMS respectively at 0.633 µm.

The model also uses the on-orbit prediction for absolute defocus: 25, 25, 65, and 30 µm for bands 1 through 4 respectively (see SDL/09-450).

Table 5: Change in Wavefront due to thermal cycling and shake. RMS at 0.633 μm

	Cryo				Shake				G-Release
	Band 1	Band 2	Band 3	Band 4	Band 1	Band 2	Band 3	Band 4	(All)
Afocal	0.09	0.09	0.09	0.09	0.06	0.06	0.06	0.06	0.178
Imager	0.07	0.07	0.07	0.07	0.11	0.11	0.11	0.11	
BSA	0.05	0.05	0.00[1]	0.00	0.24	0.24	0.12	0.12	0.0
Total	0.13	0.13	0.12	0.12	0.27	0.27	0.18	0.18	0.178

[1] Beamsplitters 2 and 3 are very stable, and the effect on bands 2, 3, and 4 is small compared to the other terms.

7.2.1 Payload

The model described in Sections 6.2.1 and 6.2.2 were used to generate a PRF using the wavefronts just described. This PRF was then convolved with the streak effects as described in Section 6.2.3. The results are listed in Table 4.

Table 6: Predicted mean image quality for the payload

	Band 1	Band 2	Band 3	Band 4
Payload	12.3	15.3	37.4	28.2
Requirement	11.8	15.4	43.3	32.8

7.2.2 Flight System

The flight system image quality was modeled using the following parameters for the spacecraft. The spacecraft has a 1.2 noise pixel requirement; the margin listed brings the spacecraft noise pixels up to its requirement[3]. The resulting flight system image quality is shown in Table 6. Note that because the payload PRF is not Gaussian, noise pixels do not add. A plot of the x-axis MTF is shown in Figure 12.

Table 7: Parameters used for flight system modeling

Parameter	Value	Unit
Roll jitter	0.6	asec (1σ)
Pitch jitter	0.9	asec (1σ)
Yaw jitter	5	asec (1σ)
Yaw misalignment	50	asec (1σ)
Pitch Rate Error	0.00006	amin/s

[3] The spacecraft CBE image quality is ~0.7 noise pixels, so this estimate is slightly conservative.

SC Margin	0.4	asec (1σ)
Pitch Rate Estimate Error	0.3	asec (1σ)

Table 8: Predicted mean image quality for the flight system

	Band 1	Band 2	Band 3	Band 4
Flight System	14.4	17.8	41.3	29.2
Requirement	14.5	18.2	48.4	34.0

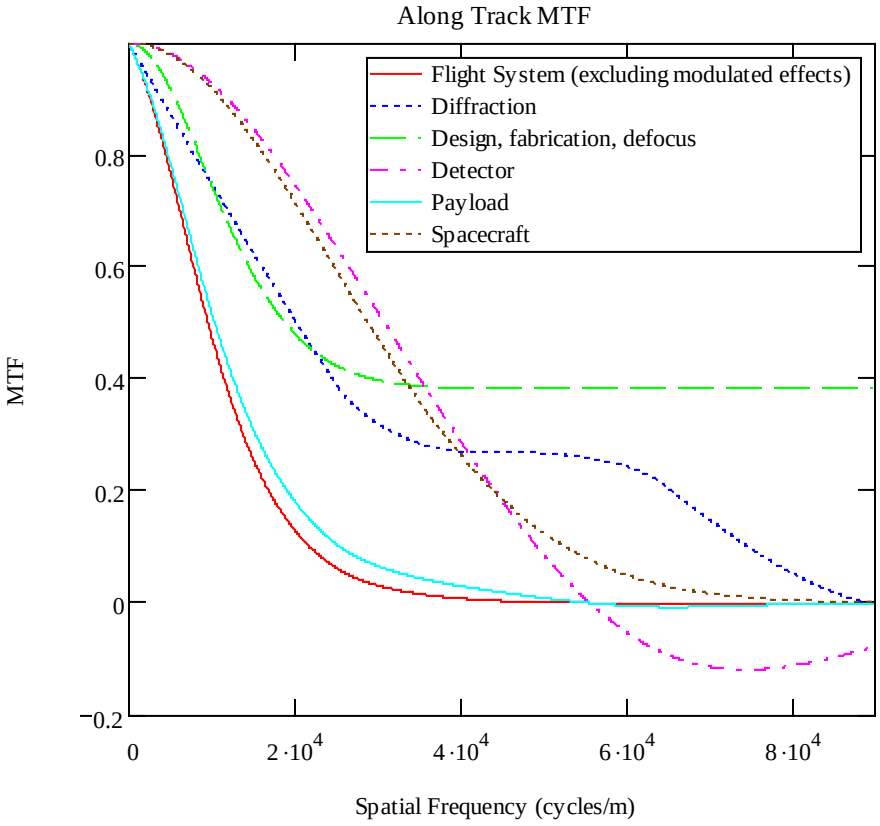

Figure 12: WISE MTF's from the parametric model.

8. CONCLUSIONS

Using surface map subtraction to compare cryo and pre- and post-vibe wavefront differences is conservative. Under these conservative assumptions, the image quality for the WISE payload meets requirements for bands 2, 3, and 4. Band 1 has a slight shortfall in payload image quality; it is predicted (conservatively) to achieve 12.4 noise pixels, slightly higher than the 11.8 noise pixel requirement.

The image quality for the flight system is predicted to meet requirements in all bands.

9. REFERENCES

1. J.D. Garnett, W.J. Forrest. “Multiply sampled read-limited and background-limited noise performance,” SPIE Vol. 1946, Infrared Detectors and Instrumentation, 1993.
2. E.L. Wright, “On Using A Space Telescope To Detect Faint Galaxies” Astronomical Society of the Pacific 97(May 1985):451-453

10. APPENDIX

The kernels discussed in Section 6.2.3 are shown in the following figures.

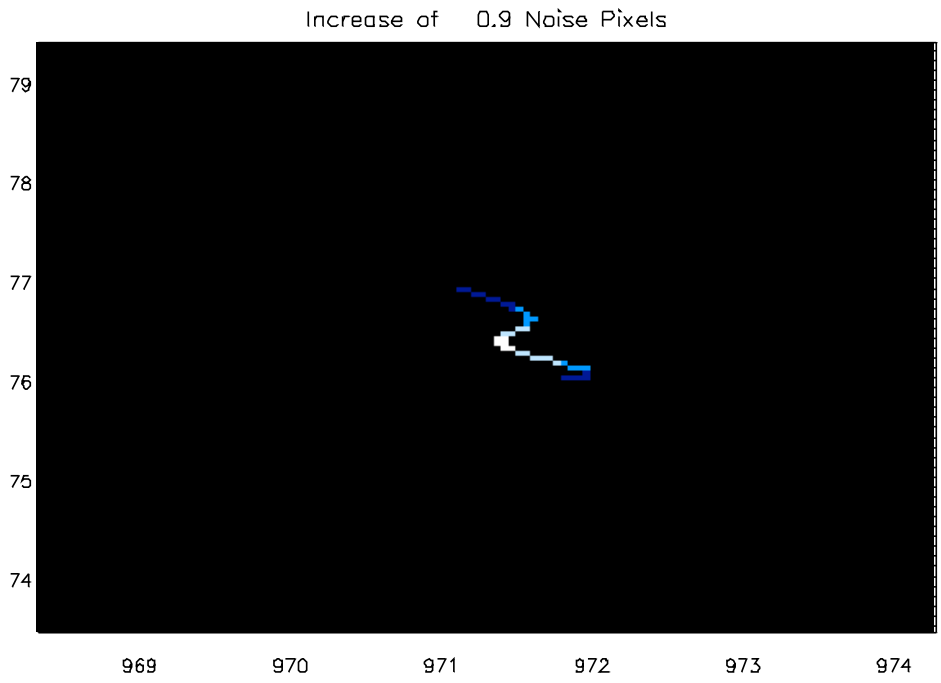
Increase of 0.9 Noise Pixels
79
78
77
76
75
74
969
970
971
972
973
974

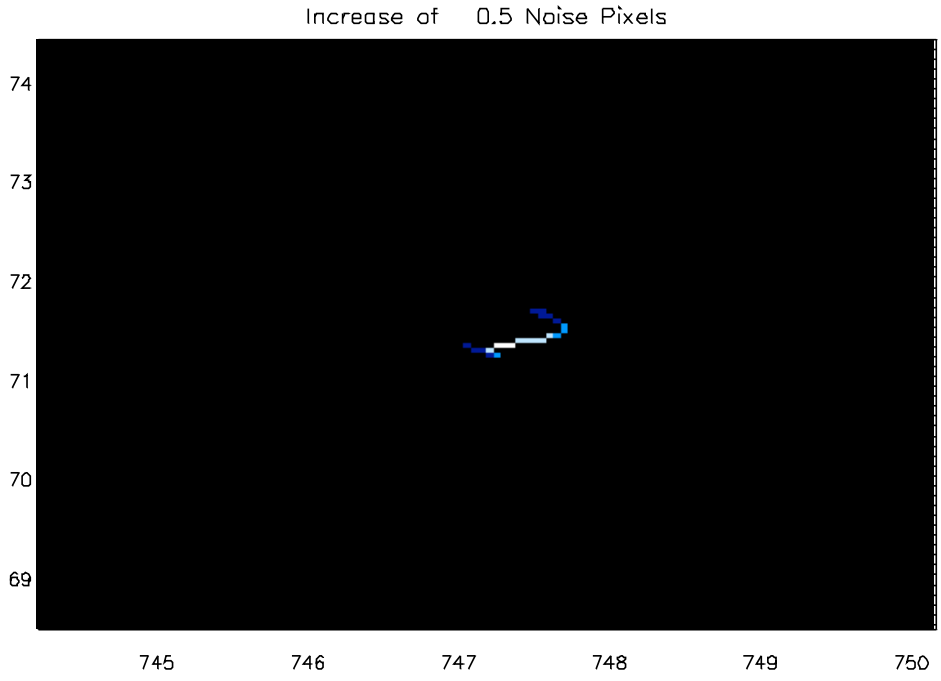
Increase of 0.5 Noise Pixels
74
73
72
71
70
69
745
746
747
748
749
750

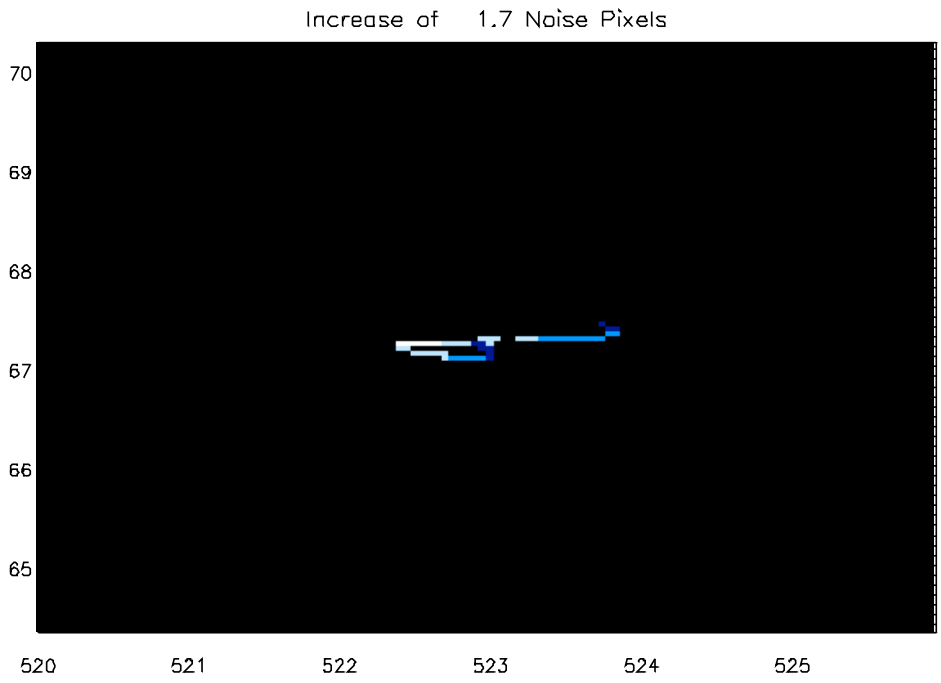
Increase of 1.7 Noise Pixels
70
69
68
67
66
65
520
521
522
523
524
525

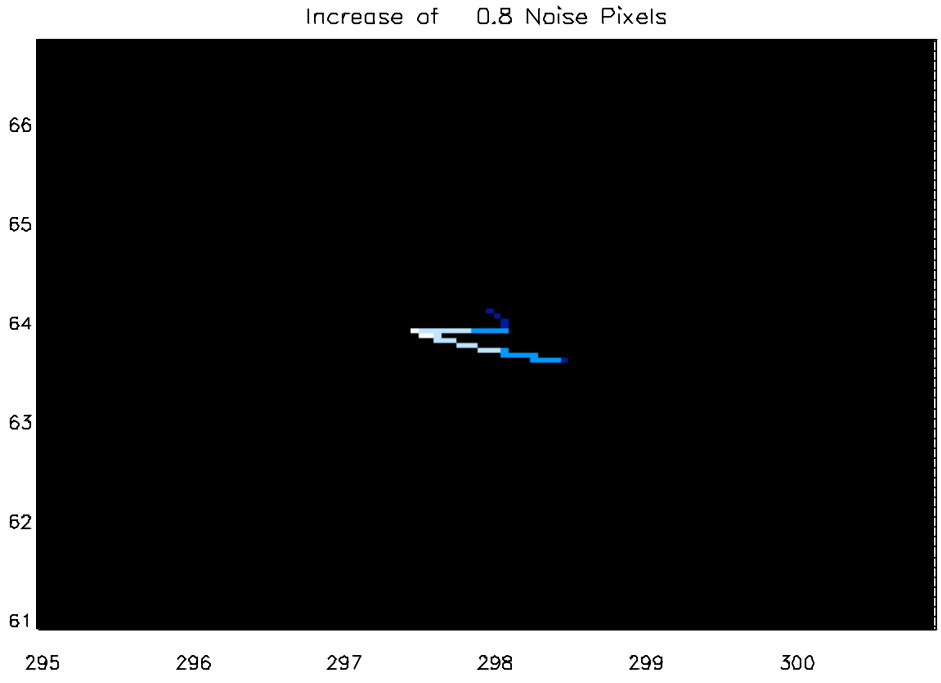
Increase of 0.8 Noise Pixels
66
65
64
63
62
61
295
296
297
298
299
300

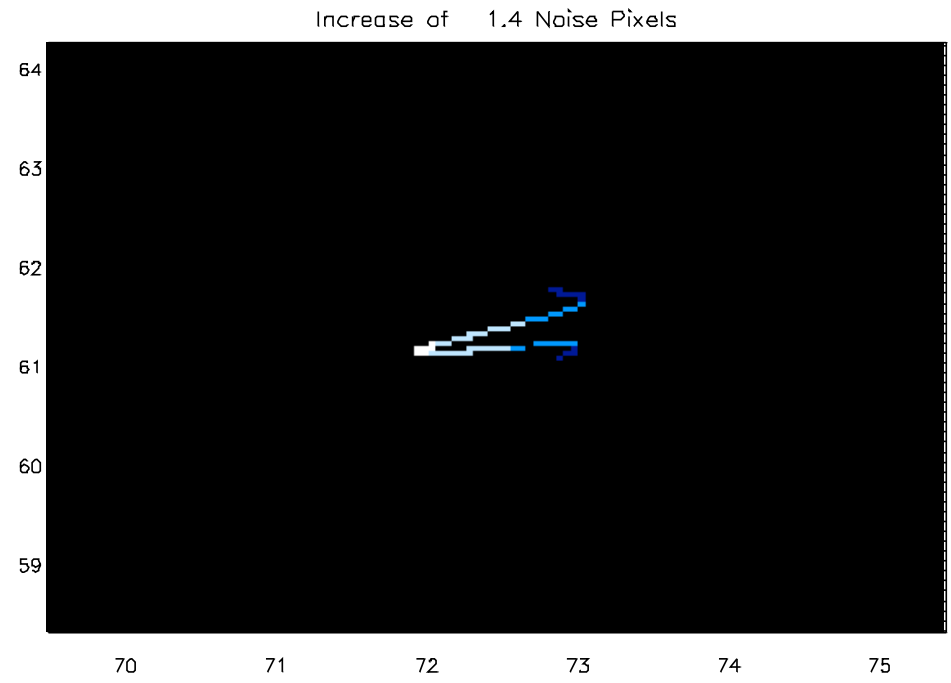
Increase of 1.4 Noise Pixels
64
63
62
61
60
59
70
71
72
73
74
75

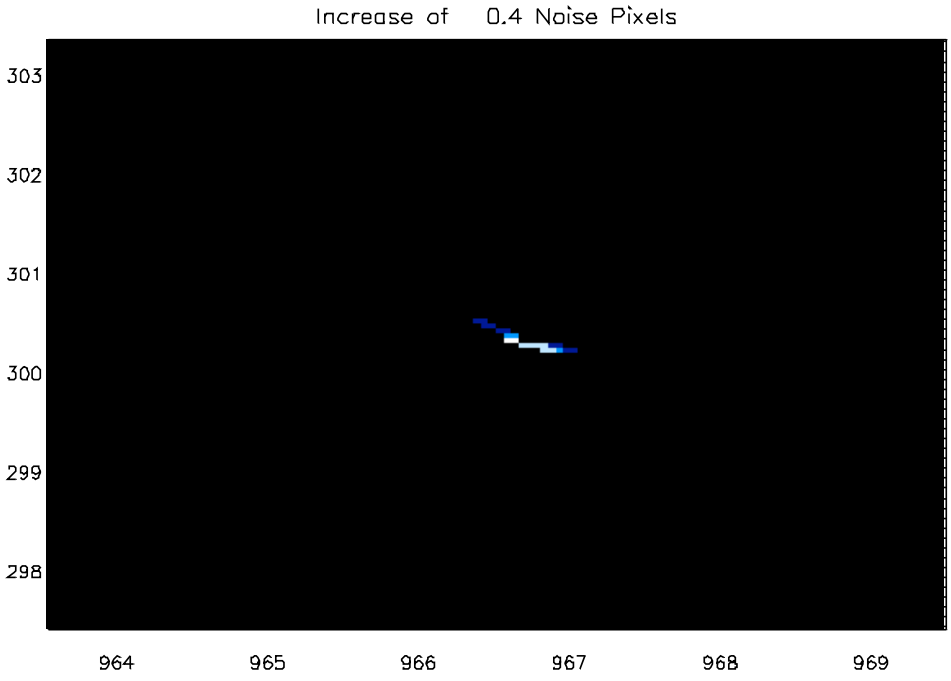
Increase of 0.4 Noise Pixels
303
302
301
300
299
298
964
965
966
967
968
969

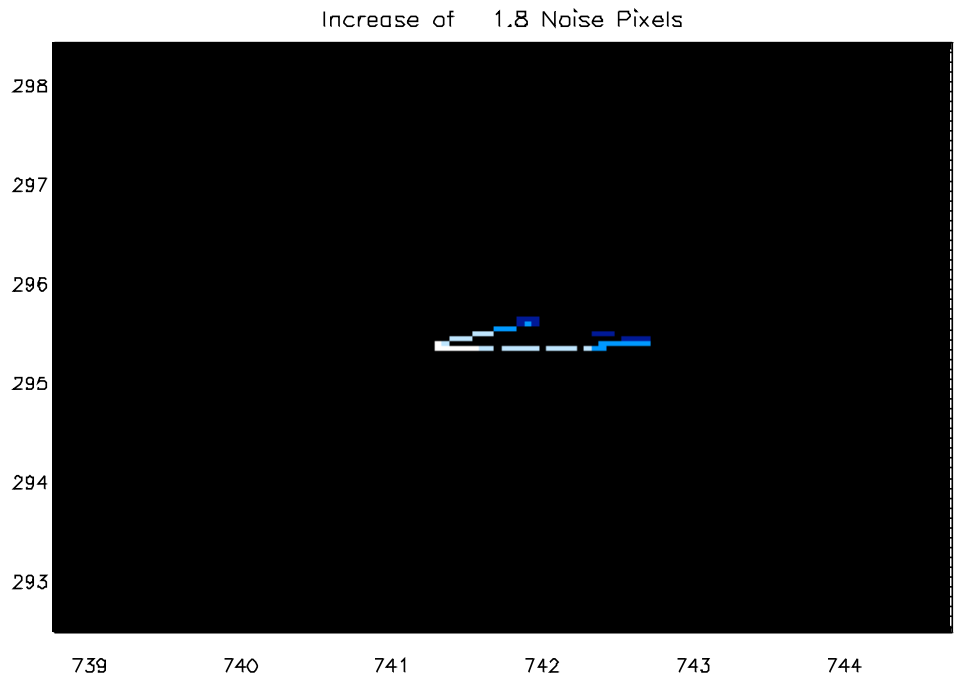
Increase of 1.8 Noise Pixels
298
297
296
295
294
293
739
740
741
742
743
744

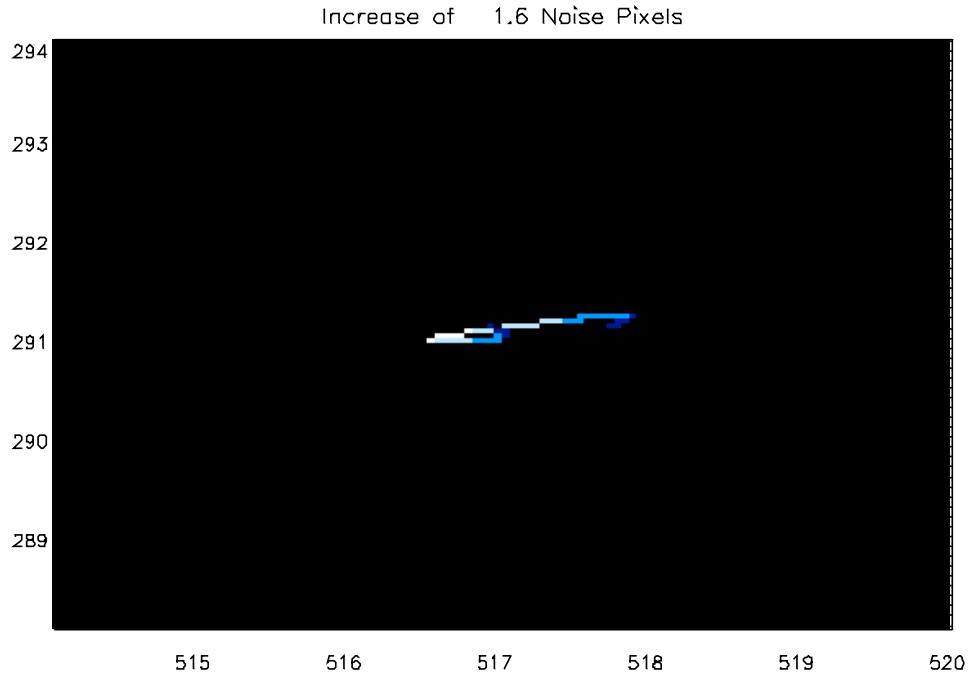
Increase of 1.6 Noise Pixels
294
293
292
291
290
289
515
516
517
518
519
520

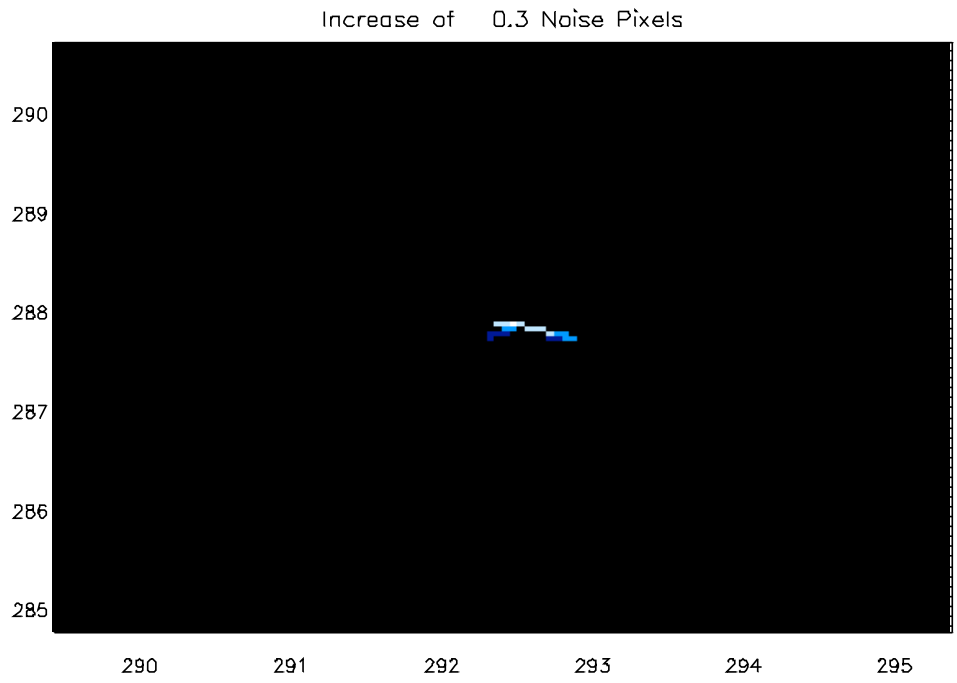
Increase of 0.3 Noise Pixels
290
289
288
287
286
285
290
291
292
293
294
295

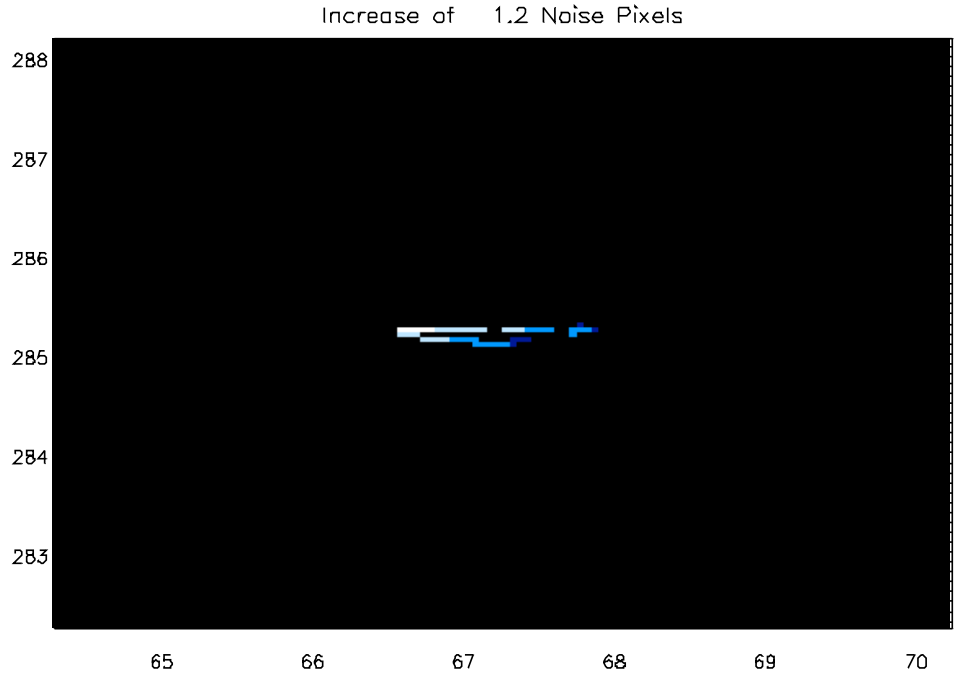
Increase of 1.2 Noise Pixels
288
287
286
285
284
283
65
66
67
68
69
70

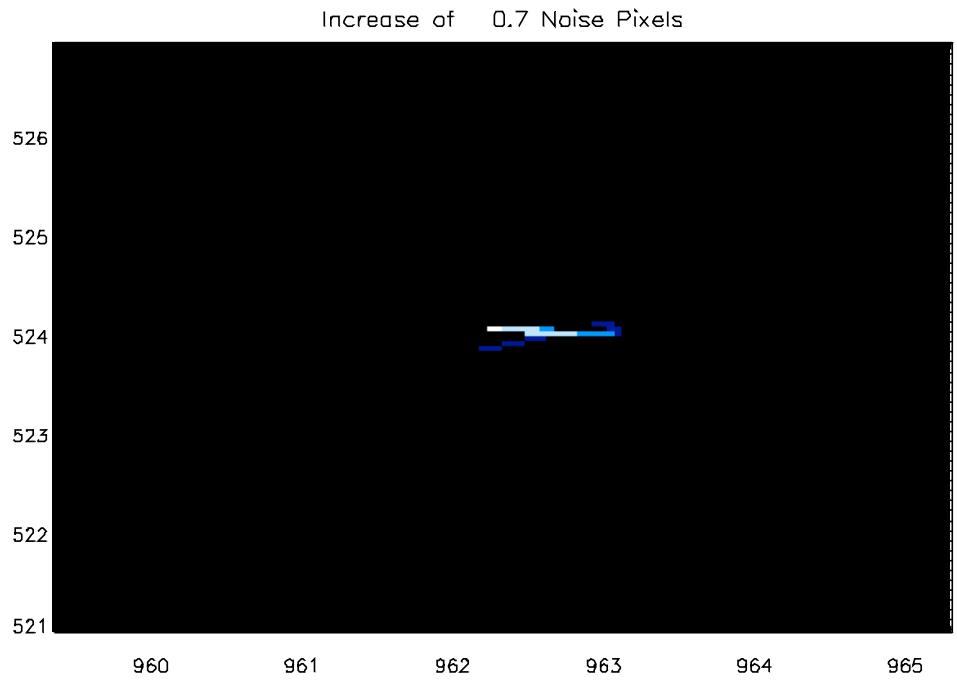
Increase of 0.7 Noise Pixels
526
525
524
523
522
521
960
961
962
963
964
965

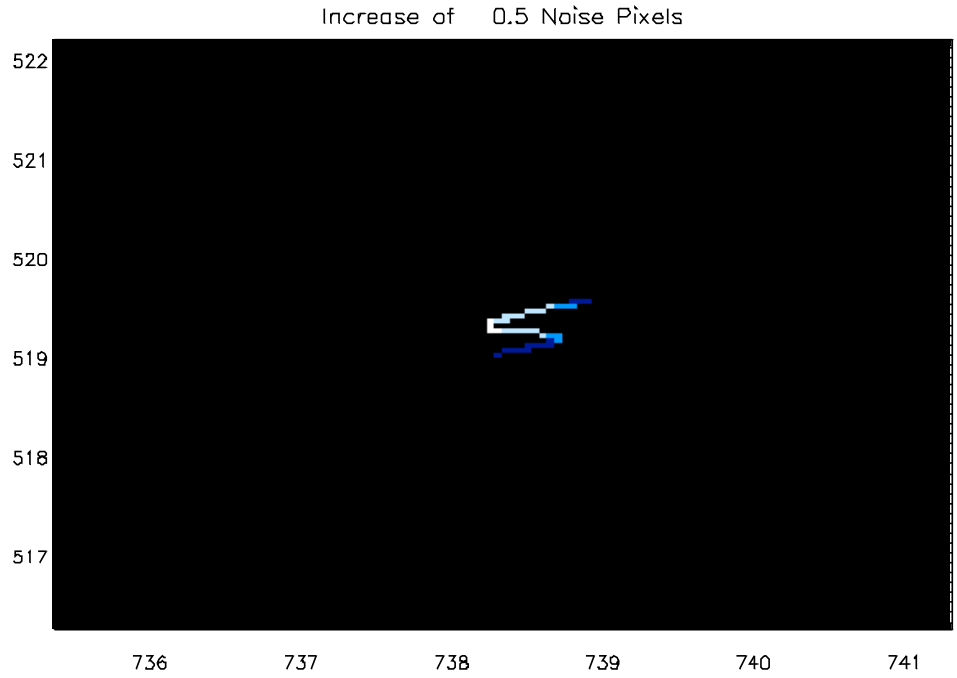
Increase of 0.5 Noise Pixels
522
521
520
519
518
517
736
737
738
739
740
741

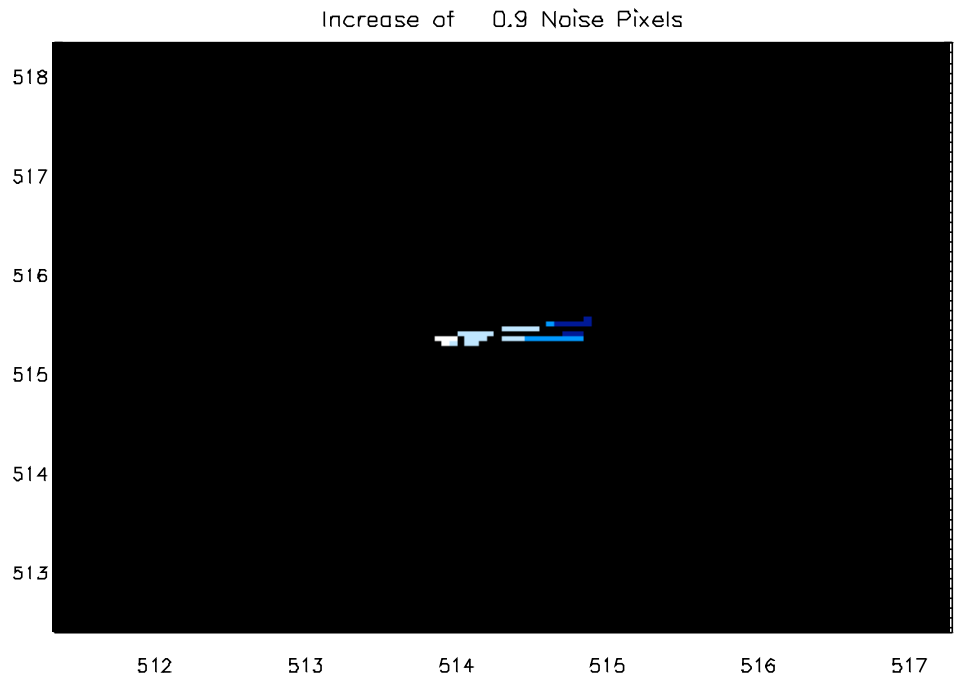
Increase of 0.9 Noise Pixels
518
517
516
515
514
513
512
513
514
515
516
517

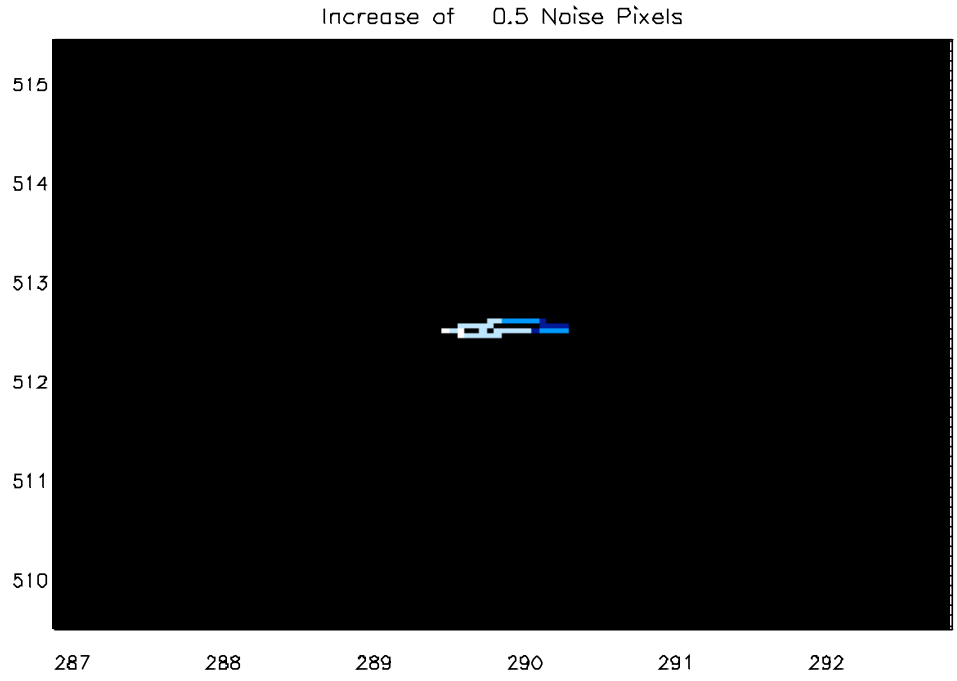
Increase of 0.5 Noise Pixels
515
514
513
512
511
510
287
288
289
290
291
292

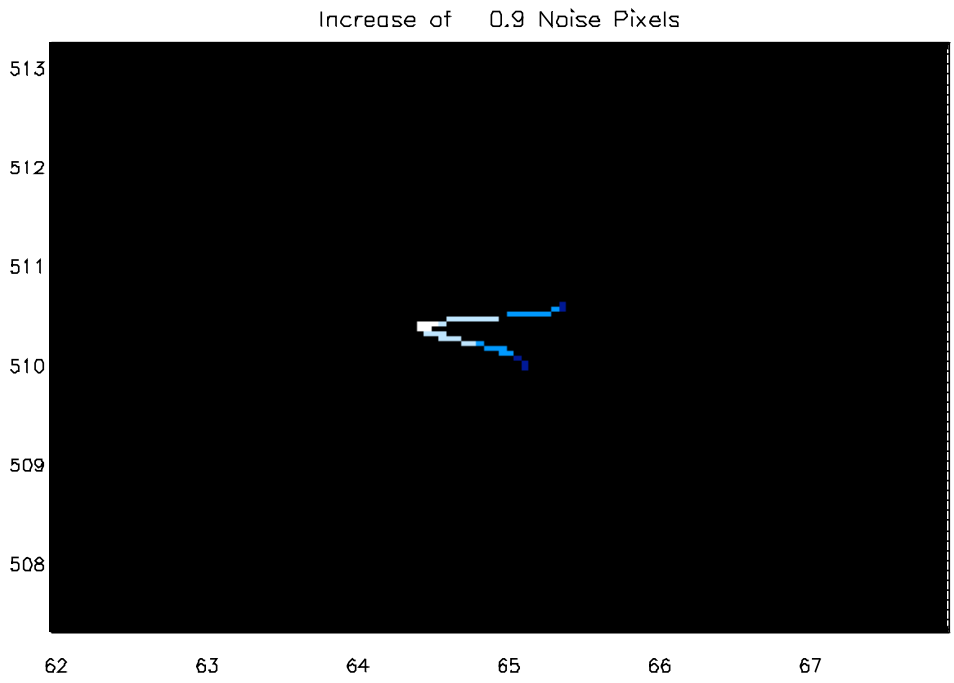
Increase of 0.9 Noise Pixels
513
512
511
510
509
508
62
63
64
65
66
67

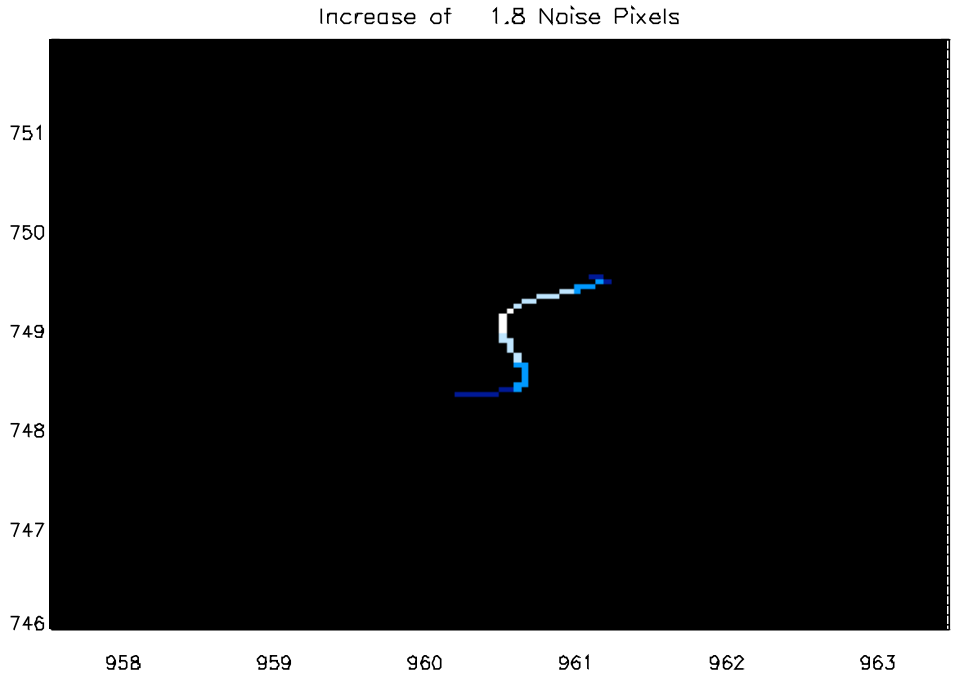
Increase of 1.8 Noise Pixels
751
750
749
748
747
746
958
959
960
961
962
963

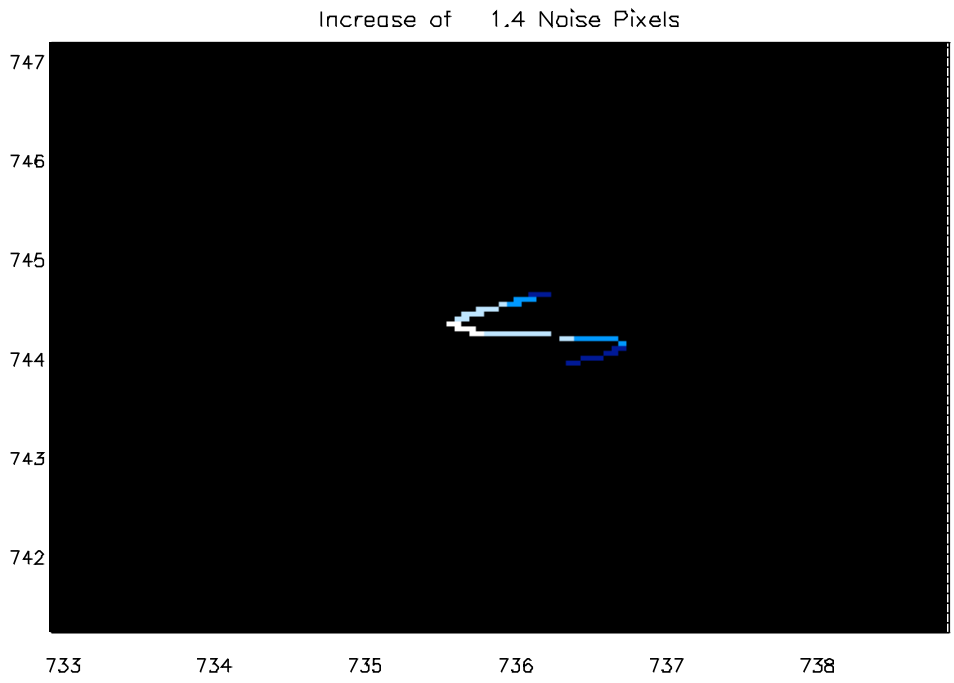
Increase of 1.4 Noise Pixels
747
746
745
744
743
742
733
734
735
736
737
738

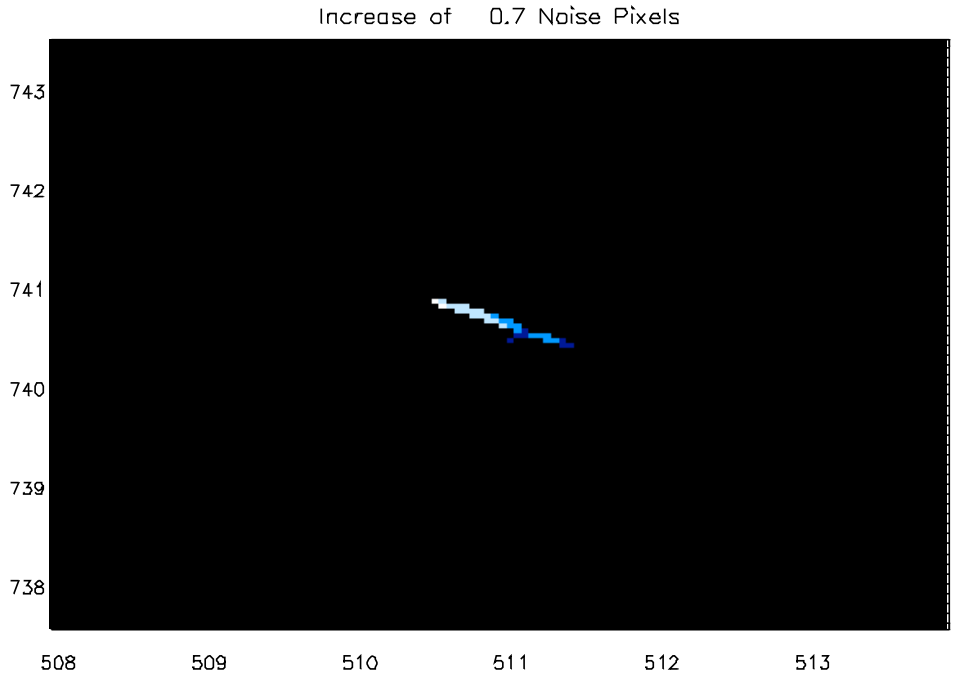
Increase of 0.7 Noise Pixels
743
742
741
740
739
738
508
509
510
511
512
513

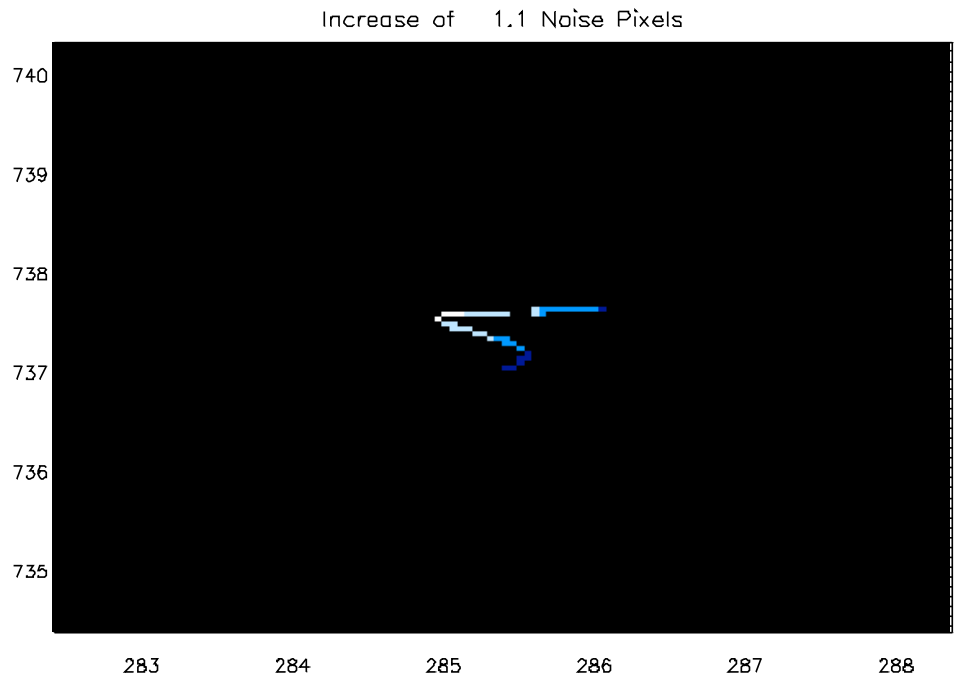
Increase of 1.1 Noise Pixels
740
739
738
737
736
735
283
284
285
286
287
288

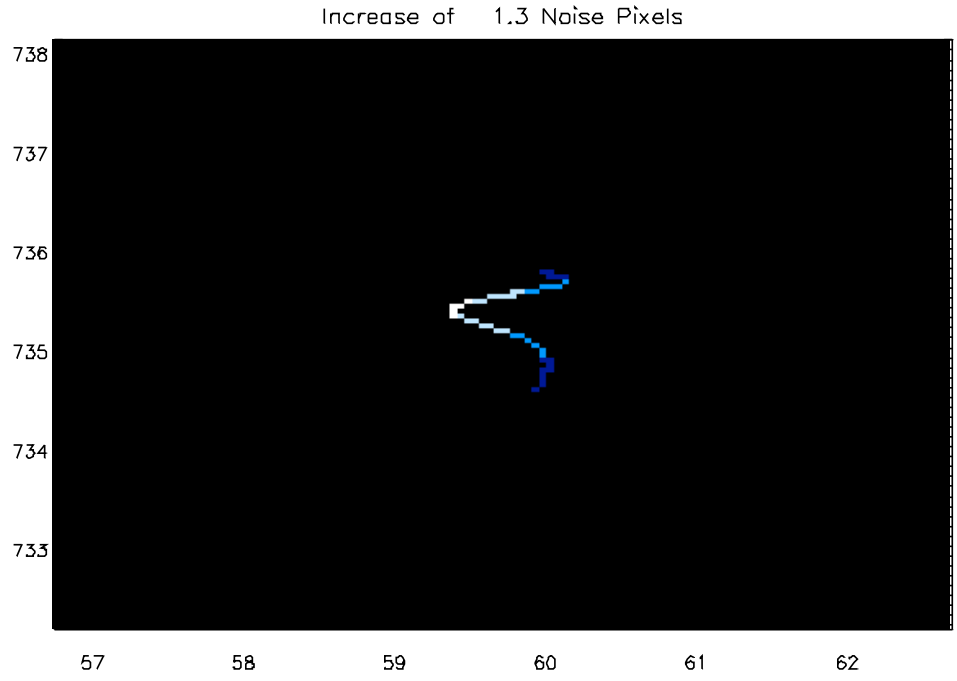
Increase of 1.3 Noise Pixels
738
737
736
735
734
733
57
58
59
60
61
62

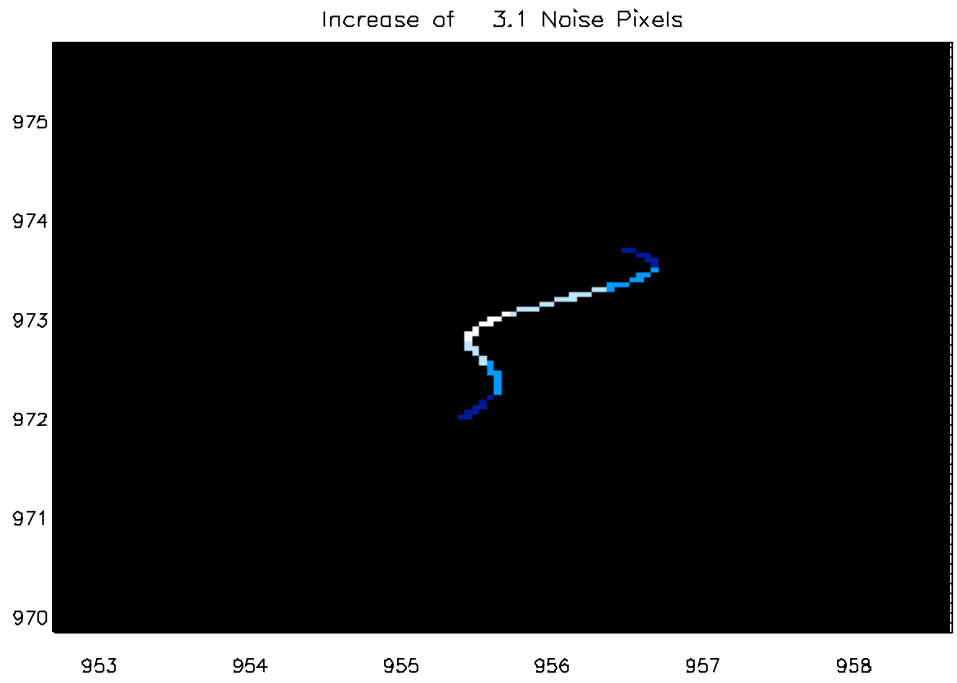
Increase of 3.1 Noise Pixels
975
974
973
972
971
970
953
954
955
956
957
958

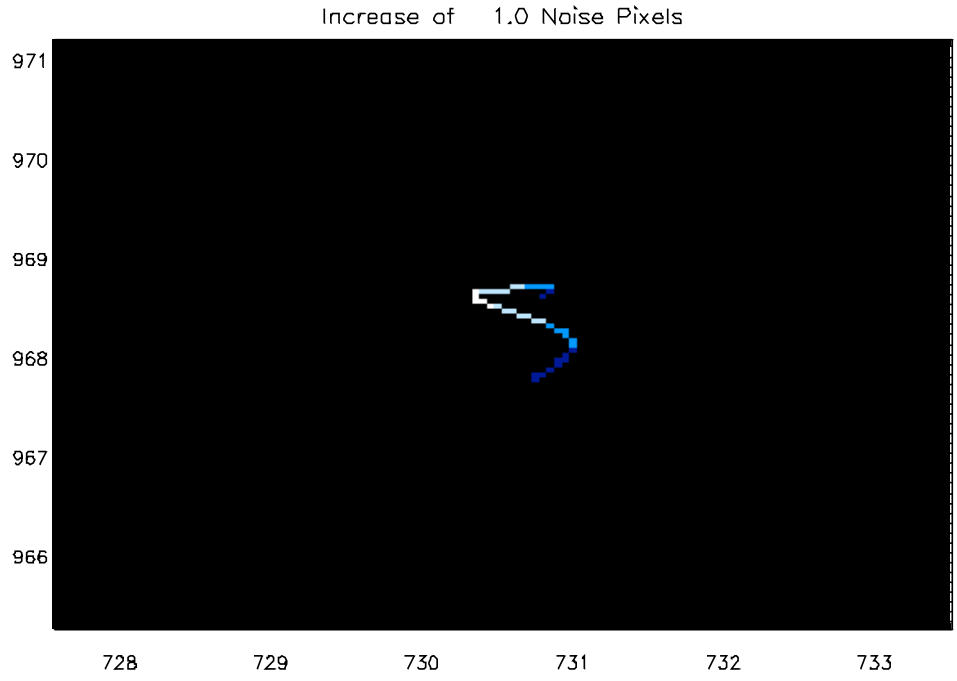
Increase of 1.0 Noise Pixels
971
970
969
968
967
966
728
729
730
731
732
733

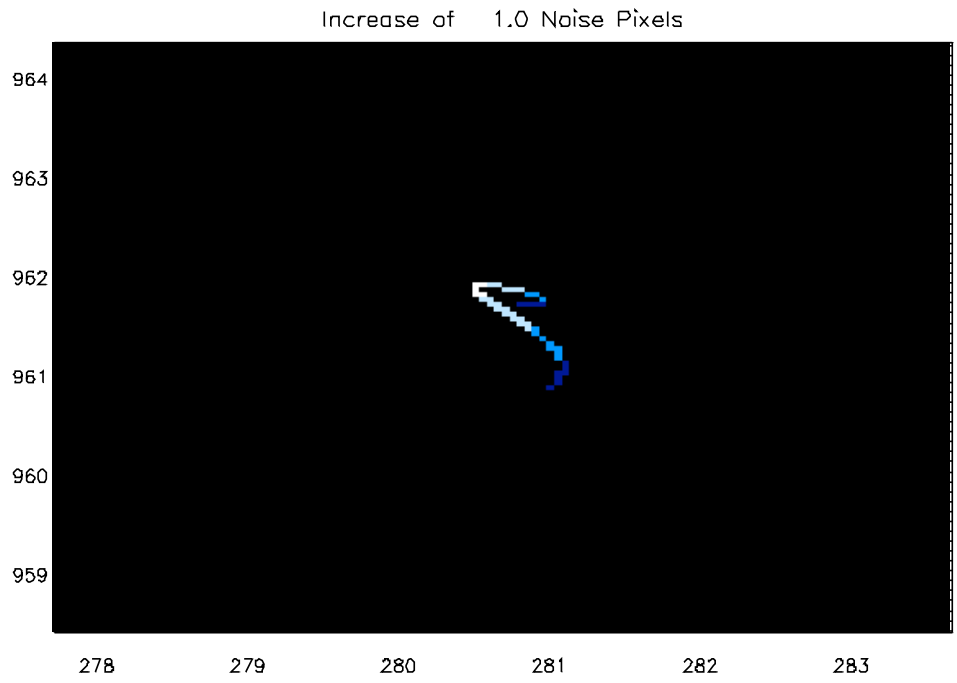
Increase of 1.0 Noise Pixels
964
963
962
961
960
959
278
279
280
281
282
283

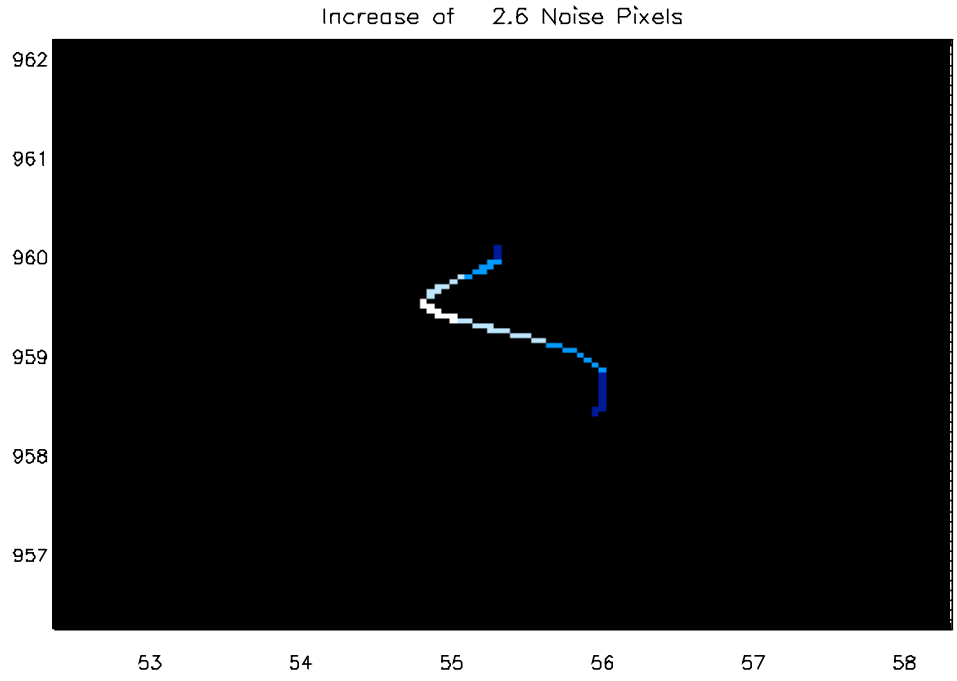
Increase of 2.6 Noise Pixels
962
961
960
959
958
957
53
54
55
56
57
58